RESEARCH ARTICLE

Facile synthesis of rapamycin-loaded PEG-*b*-PLA nanoparticles and their application in immunotherapy

Yudong Li[1] | Jari F. Scheerstra[1] | Yuechi Liu[1] | Annelies C. Wauters[1,2,3] |
Jianhong Wang[1] | Hanglong Wu[1] | Tania Patiño[1] |
Antoni Llopis-Lorente[1] | Jan C. M. van Hest[1] | Loai K. E. A. Abdelmohsen[1]

[1]Bio-Organic Chemistry, Institute for Complex Molecular Systems, Eindhoven University of Technology, Eindhoven, The Netherlands

[2]Department of Tumor Immunology, Radboud Institute for Molecular Life Sciences, Radboud University Medical Center, Nijmegen, The Netherlands

[3]Division of Immunotherapy, Oncode Institute, Radboud University Medical Center, Nijmegen, The Netherlands

Correspondence
Loai K. E. A. Abdelmohsen, Jan C. M. van Hest, and Antoni Llopis-Lorente, Bio-Organic Chemistry, Institute for Complex Molecular Systems, Eindhoven University of Technology, P.O. Box 513, 5600 MB, Eindhoven, The Netherlands.
Email: l.k.e.a.abdelmohsen@tue.nl; j.c.m.v.hest@tue.nl; anllolo2@upvnet.upv.es

Present address
Antoni Llopis-Lorente, Institute of Molecular Recognition and Technological Development (IDM); CIBER de Bioingeniería, Biomateriales y Nanomedicina (CIBER-BBN), Universitat Politècnica de València, Valencia, Spain.

Funding information
European Commission, Grant/Award Number: 694120

Abstract

Poly(ethylene glycol)-block-poly(lactide) (PEG-*b*-PLA) micro- and nanoparticles (NPs) have been intensively investigated for applications in biomedicine, due to their inherent biocompatibility and biodegradability, which allows them to be used as sustained release systems. Current methods for preparing PEG-*b*-PLA NPs typically require two different steps that include polymer synthesis and NP assembly, with the necessary intermediate polymer purification and the use of a variety of organic solvents in the process. In order to facilitate the biomedical application of PEG-*b*-PLA NPs, it is of great interest to develop a strategy to formulate the NPs in a simplified manner. Here, we report a straightforward method to construct PEG-*b*-PLA NPs through a sequential two-step process without intermediate work-up, which involves synthesizing the polymer in a water-miscible organic solvent that is, *N,N*-dimethylformamide (DMF), followed by addition of water to the polymer solution. In this way, large NPs (~600 nm) were prepared. We comprehensively characterized the NPs using turbidity studies, dynamic light scattering (DLS), scanning electron microscopy (SEM), and transmission electron microscopy (TEM) techniques. We further demonstrated the ability of the NPs to encapsulate drugs, exemplified in the immunotherapeutic agent rapamycin, with relatively high encapsulation efficiency. In vitro drug release tests showed that rapamycin-encapsulating NPs had comparable sustained-release profiles at different pH conditions, highlighting the broad application window of our NP platform. Moreover, in vitro T cell suppression assays revealed that rapamycin-loaded NPs exhibited similar inhibitory performance to free rapamycin on

Yudong Li and Jari F. Scheerstra contributed equally to this work and share first authorship.

CD8$^+$ cells at all rapamycin concentrations and on CD4$^+$ cells at high and intermediate rapamycin concentrations, while the performance of the NPs was superior on CD4$^+$ at low rapamycin concentration. Overall, this work provides a route for the scalable synthesis of biocompatible PEG-*b*-PLA NPs, which can be extended to other polymeric NPs, with potential in biomedical applications such as immunotherapy.

KEYWORDS

immunotherapy, nanoparticles, PEG-b-PLA, self-assembly

1 | INTRODUCTION

Polymeric micro- and nanoparticles (NPs) are an important class of nanomedicines, because of their structural properties, which can be easily customized and replicated on demand—especially when compared to their lipid counterparts. The development of polymeric NPs in terms of their architectures and functions, including shape, size, surface modification, and cargo encapsulation, has advanced rapidly over the past decades.[1] In turn, they have been utilized in a variety of biomedical applications, including diagnosis and treatment of diseases.[2] In this regard, poly(ethylene glycol)-block-poly(lactide) (PEG-*b*-PLA)-based NPs are of particular interest due to their biocompatibility and biodegradability.[3–5] Although there have been numerous studies on the preparation of different kinds of PEG-*b*-PLA NPs, for instance, nanospheres, micelles and vesicles, there are key challenges remaining, such as obtaining control over particle nanostructure, size, and morphology; and improving the preparation efficiency.

The current methods for preparing PEG-*b*-PLA NPs generally require two main steps, that is, polymer synthesis and particle assembly (and corresponding intermediate work-up steps). These two steps are traditionally not integrated, not only because polymer purification is needed after synthesis, but also because the solvents required for the two steps are often different. For example, dichloromethane (DCM) is a commonly used solvent in the organocatalytic ring-opening polymerization of lactide.[6–9] However, DCM is not a preferred solvent for particle formation by self-assembly of amphiphilic polymers induced by solvent switching, because of its immiscibility with water. Nevertheless, utilizing DCM, PEG-*b*-PLA particles can be generated by emulsion and subsequent evaporation—yet, the resulting particles are typically larger than 1 μm in diameter,[10–12] which restrains their use in the biomedical field. Therefore, water-miscible solvents, such as *N*,*N*-dimethylformamide (DMF),[13] acetone,[14] tetrahydrofuran (THF) and dioxane,[6]

are more popular choices for self-assembly of such amphiphilic polymers, and the particle size can be tuned in the range of a few to hundreds of nanometers, which is considered to be necessary for applications such as drug delivery.

One approach to improve current limitations and explore the continuous preparation of polymeric NPs directly from their starting materials is to use only one solvent for polymer synthesis and particle assembly. In this context, polymerization-induced self-assembly (PISA) has been developed. PISA is an effective and versatile technique to synthesize polymeric NPs while allowing encapsulation of cargos during the process. The advantages of this technique include facile control over the morphology and size of NPs, as well as high loading efficiency.[15,16] Despite many efforts along this direction to prepare polyester-based NPs, the difficulties remain due to lack of proper monomer/polymer/solvent combinations, and only a few cases have been reported so far.[17,18] By a combination of ring-opening PISA with crystallization-driven self-assembly (CDSA), named ROPI-CDSA, PEG-*b*-PLA nanostructures with various morphologies were achieved from a PEG-based initiator and lactide.[17] However, such methodology is relatively time-consuming due to the slow rate of the self-assembly step, which typically requires several hours or even days. Alternatively, solvent-switched self-assembly of the polymer directly after synthesis could pave the way for high-throughput preparation of PEG-*b*-PLA NPs. This can be achieved by adding water to the organic solvent used for polymer synthesis. However, such a system requires elaborate design, especially the choice of organic solvent, as it has an impact on both polymer synthesis and particle assembly steps, such as monomer conversion and microphase separation behavior of the solution.

Rapamycin, also known as sirolimus, is a hydrophobic immunosuppressive drug that inhibits or prevents organ transplant rejection and has been used in clinical trials since the end of the last century.[19,20] However, rapamycin has poor water solubility, limited
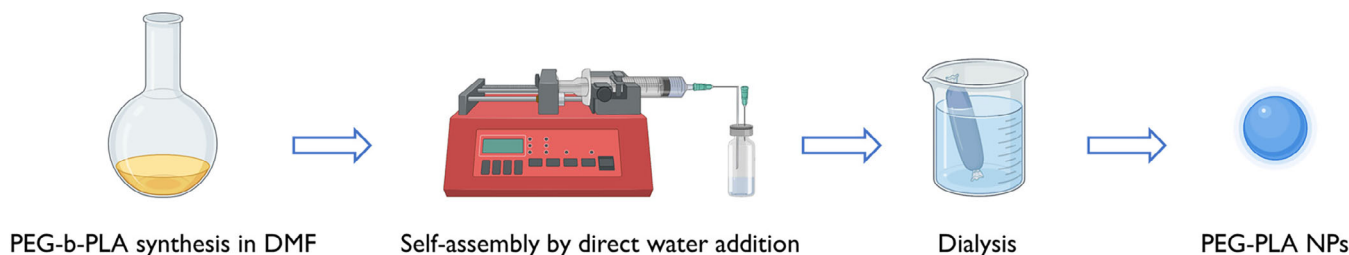
FIGURE 1 Schematic of the continuous process for the preparation of PEG-*b*-PLA nanoparticles (NPs). First, PEG-*b*-PLA block copolymer was synthesized in dry *N,N*-dimethylformamide (DMF). After that, the PEG-*b*-PLA solution was further diluted with DMF, and then water was slowly dropped into the solution to induce the self-assembly of the polymer, thereby forming PEG-*b*-PLA NPs. Finally, dialysis was performed to remove DMF, catalyst, and unreacted monomers. For the preparation of rapamycin-loaded NPs, rapamycin was added during the diluting step with DMF. After dialysis, residual rapamycin was removed by centrifugation.
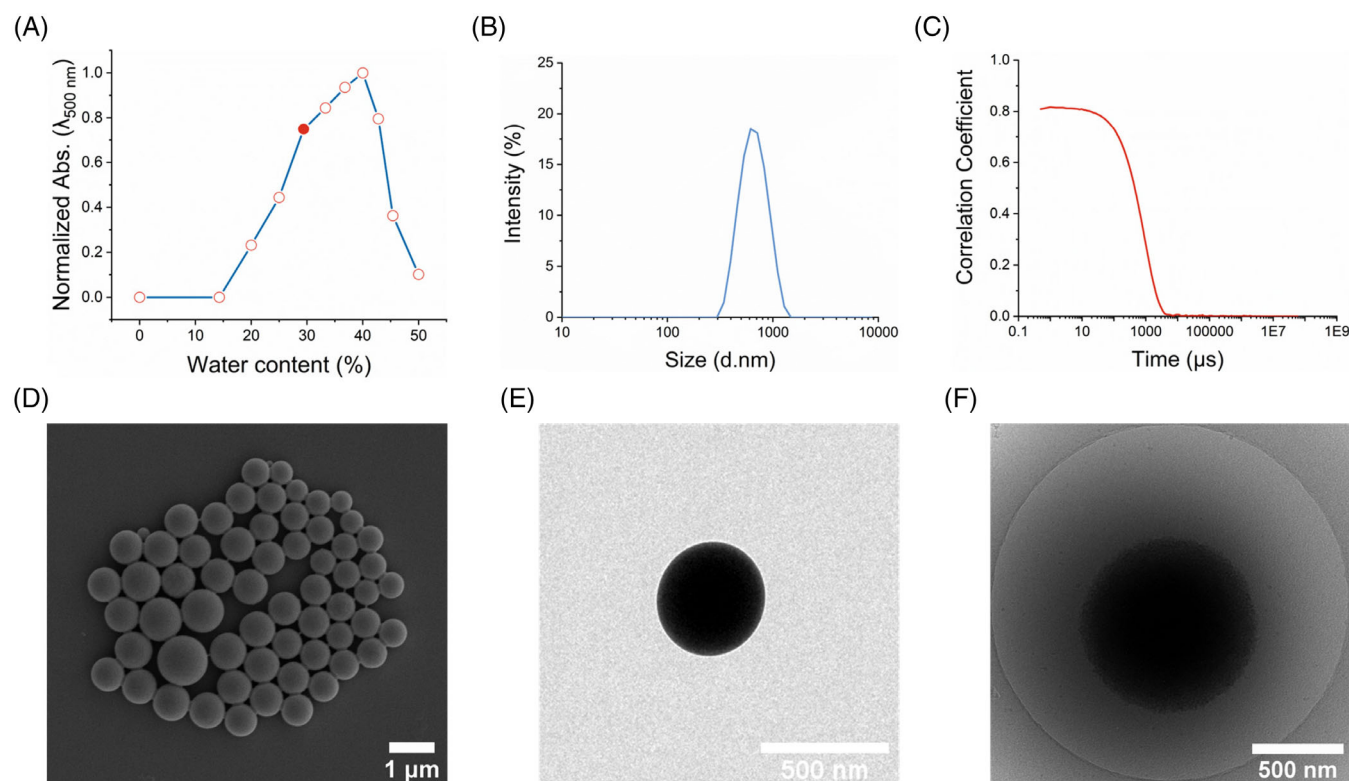
FIGURE 2 Characterization of PEG-*b*-PLA nanoparticles (NPs). (A) Normalized turbidity measurements of PEG-*b*-PLA block copolymer in DMF upon water addition (C_w: 0–50 vol%). 29 vol% was chosen as C_w for particle formation followed by dialysis: dynamic light scattering (DLS) data showing both (B) intensity profile indicating D_h distribution and (C) correlogram of NPs; representative microscopy images of NPs acquired by (D) SEM, (E) dry-transmission electron microscopy (TEM), and (F) cryo-TEM.

bioavailability as well as high repeat-dose toxicity,[21] making it difficult to be administered systemically in its free form. Therefore, the use of rapamycin-loaded carriers that can provide a sustained release of the drug represents a solution to these problems, whilst providing synergistically enhanced therapeutic benefits.[22,23]

In this study, we demonstrate an approach to sequentially synthesize amphiphilic copolymers and directly induce their assembly, without the need of polymer purification or switching of solvents, eliminating unnecessary

time-consuming additional steps. To this end, PEG-*b*-PLA block copolymer was synthesized in dry DMF instead of the commonly used solvent, dry DCM. Thereafter, the PEG-*b*-PLA solution was further diluted with DMF, and then water was slowly dropped into the solution to induce the self-assembly of the polymer, which led to the formation of PEG-*b*-PLA NPs. Finally, dialysis was performed to remove DMF, catalyst, and unreacted monomers (Figure 1). This resulted in a NP solution, which was subsequently characterized by dynamic light scattering

(DLS), scanning electron microscopy (SEM), and transmission electron microscopy (dry-TEM and cryo-TEM) techniques (Figure 2). The NPs had an average size of ca. 600 nm, and polydispersity index (PDI) below 0.1. Furthermore, the potential drug delivery capacity of PEG-*b*-PLA NPs was investigated by encapsulating rapamycin and demonstrating its release. In vitro drug release tests showed that rapamycin-loaded NPs exhibited comparable sustained-release profiles at different pH conditions, which could be elucidated by the similarity in the degradation behavior of the NP matrix during release. In addition, in vitro T cell suppression assays showed that rapamycin-loaded NPs did not impair the inhibitory performance on CD8$^+$ cells at all rapamycin concentrations compared to free rapamycin. As for the inhibition on CD4$^+$ cells, the loaded NPs also showed similar performance to free rapamycin at high and medium rapamycin concentrations, while they even exhibited better performance at low rapamycin concentration.

2 | EXPERIMENTAL SECTION

2.1 | Materials

All materials were used as received without further purification unless otherwise indicated. α-methoxy-ω-hydroxy polyethylene glycol (mPEG, average M_n 1 kDa, 95%) was purchased from Biopharma PEG Scientific (Biochempeg Scientific). *N,N*-dimethylformamide (DMF), tetrahydrofuran (THF) and dioxane were obtained from Biosolve Chimie. Rapamycin (98%) was supplied by Adooq Bioscience. 3,6-dimethyl-1,4-dioxane-2,5-dione (D,L-lactide, 99%), 1,8-diazabicyclo[5.4.0]undec-7-ene (DBU, 98%) and all other chemicals were obtained from Sigma-Aldrich unless otherwise stated. Dialysis membranes (MWCO: 3.5 and 12–14 kDa, Spectra/Pro$^®$) were used for polymer and NP purification, respectively. Water used in this work was ultrapure Milli-Q (Millipore) water (18.2 MΩ cm).

2.2 | Instruments

2.2.1 | Nuclear magnetic resonance spectroscopy

Proton nuclear magnetic resonance (^{1}H-NMR) measurements were conducted on a Bruker Avance 400 MHz Ultrashield spectrometer equipped with a Bruker SampleCase autosampler, using CDCl$_3$ as the solvent and TMS as the internal standard. The obtained spectra were analyzed using MestReNova NMR analysis software.

2.2.2 | Gel permeation chromatography

The molecular weights and dispersity (Đ) of the copolymers were characterized by using a Prominence-I gel permeation chromatography (GPC) system (Shimadzu) equipped with a PL gel 5 μm mixed D (Polymer Laboratories) and differential refractive index (RI) and ultraviolet (UV) detectors. THF was used as the eluent with a flow rate of 1 mL per minute. Polystyrene standards (Polymer Laboratories) were used for calibration. GPC chromatograms for polymer analysis were obtained from the RI detector, and GPC chromatograms for rapamycin analysis were obtained from the UV detector.

2.2.3 | DLS and zeta potential (ζ) measurements

The hydrodynamic diameter (D_h), polydispersity index (PDI), and zeta potential (ζ) of the NPs were measured using a Malvern Instruments Zetasizer (model Nano ZSP) equipped with a 633 nm He-Ne laser and an avalanche photodiode detector at 25°C, using a ZEN0040 type disposable cuvette cell (100 μL sample volume). Zetasizer software was used to process and analyze the data.

2.2.4 | Ultraviolet–visible spectroscopy

Ultraviolet–visible (UV–Vis) spectra were recorded with a Cary 3500 Multicell UV–Vis spectrophotometer (Agilent Technologies) using a quartz cuvette (1 mL sample volume).

2.2.5 | Fluorescence spectroscopy

Fluorescence intensity measurements were performed on a Spark multimode microplate reader (Tecan).

2.2.6 | Scanning electron microscopy

Particle morphology was assessed by scanning electron microscopy (SEM) (FEI Quanta 200 3D FEG).

2.2.7 | Transmission electron microscopy

Dry-transmission electron microscopy (TEM) images were recorded on a FEI Tecnai 20 (type Sphera) at 200 kV. Samples for dry-TEM were prepared by dropping 20 μL of samples (ca. 2.3 mg/mL) onto a carbon-coated

copper grid. The samples were dried at room temperature.

2.2.8 | Cryogenic transmission electron microscopy

Cryogenic transmission electron microscopy (cryo-TEM) experiments were performed on the TU/e CryoTitan (Thermo Fisher Scientific) equipped with a field emission gun and autoloader and operated at 300 kV acceleration voltage in low-dose bright-field TEM mode. Samples for cryo-TEM were prepared by glow discharging the grids (Quantifoil Cu grid with R 2/2 holey carbon films, Quantifoil Micro Tools GmbH, part of the SPT Life Sciences group) in a Cressington 208 carbon coater for 40 s. Then, 3 μL of samples (ca. 2.3 mg/mL) was pipetted on the grid and blotted in a Vitrobot MARK IV at room temperature and 100% humidity. The grid was blotted for 3 s (offset −3) and directly plunged and vitrified in liquid ethane. Cryo-TEM images were acquired in zero loss energy filtering mode (Gatan GIF 2002, 20 eV energy slit) with a CCD camera (Gatan model 794). Processing of all electron microscope images was performed with Fiji 2.7.0 software (ImageJ2).[24]

2.2.9 | Gas chromatography with flame ionization detection

Gas chromatography with flame ionization detection (GC-FID) measurements were performed on a Shimadzu GC-2010 system equipped with an autosampler with a Zebron ZB-FFAP GC Column of 30 m × 0.25 mm × 0.25 μm and using the following temperature program: 130°C|10 min.

2.2.10 | pH meter

FiveEasy Plus FP20 pH Meter (Mettler Toledo) was used to monitor the pH.

2.2.11 | Freeze-dryer

Lyophilization was performed on an Alpha 2–4 LSCbasic freeze-dryer (Christ).

2.2.12 | Centrifuge

Centrifugation was carried out on a Eppendof 5424R microcentrifuge.

2.3 | Methods

2.3.1 | Synthesis and characterization of PEG-b-PLA block copolymer

The synthesis of PEG-b-PLA was performed according to a previously reported procedure with several modifications.[6] To synthesize copolymer with composition of PEG_{22}-b-PLA_{45}, 97 mg (0.1 mmol) of $mPEG_{22}$ and 650 mg (4.5 mmol, 45 equiv.) of D,L-lactide were first weighed in a 250-mL round-bottom flask. Subsequently, dry toluene (ca. 50 mL) was added to the flask and the solvent was evaporated to dry the contents before polymerization. The dried reagents were then re-dissolved in dry DMF (5.62 mL, [monomer] = 0.8 M) and DBU was added (0.5 equiv. with respect to [initiator]; 0.05 mmol) under argon. The reaction proceeded with magnetic stirring at room temperature. The progress of the reaction was monitored by ^{1}H-NMR spectroscopy until the monomer conversion exceeded 95%. In a typical reaction, it reached this point within 4 h. After that, the solution was taken out and the polymer concentration was calculated according to the following equation:

$$\text{Conc}_{\text{PEG}-b-\text{PLA}} = \frac{W_{\text{mPEG}} + W_{\text{D,L−lactide}} \times \text{Monomer conversion}}{V_{\text{after reaction}}}$$

(1)

with $\text{Conc}_{\text{PEG}-b-\text{PLA}}$ the concentration of PEG-b-PLA block copolymer in DMF after the reaction, $W_{m\text{PEG}}$ the weight of the mPEG, $W_{\text{D,L−lactide}}$ the weight of D,L-lactide, $V_{\text{after reaction}}$ the volume of the solution after the reaction (typically ca. 6.2 mL).

To characterize the synthesized polymer, 300 μL of the solution was directly transferred to a prehydrated dialysis tube (MWCO: 3.5 kDa). Dialysis was performed against precooled water at 4°C for 24 h with frequent water changes. After dialysis, the solution was lyophilized to yield a white powder (yield = 76%). The synthesized copolymer was characterized using ^{1}H NMR spectroscopy and GPC to determine copolymer composition and polydispersity, respectively. ^{1}H-NMR (CDCl$_3$, 400 MHz, δ in ppm): 5.28–5.10 ppm (m, PLA C**H**), 3.64 ppm (s, PEG backbone C**H$_2$**), 3.38 ppm (s, PEG C**H$_3$**O), 1.65–1.45 ppm (m, PLA C**H$_3$**).

2.3.2 | Investigation of PEG-b-PLA self-assembly by turbidity studies

After determining the polymer concentration according to Equation (1), the solution of PEG-b-PLA was first diluted with DMF to a concentration of 10 mg/mL. Next, different volumes of water were added to 1 mL of the

polymer solution at a constant rate (1 mL/h) via a syringe pump under stirring at 700 rpm. When the time reached 10, 15, 20, 25, 30, 35, 40, 45, 50, 60 min (corresponding to volumetric water content of 14%, 20%, 25%, 29%, 33%, 37%, 40%, 43%, 45%, and 50%), the pump was manually stopped and the dispersion was stirred for several additional minutes. Subsequently, the turbidities were recorded by a UV–Vis spectrophotometer at a wavelength of 500 nm. DMF was used as the reference for all the measurements. Similarly, the turbidity studies with THF and dioxane as organic solvents were conducted.

2.3.3 | Preparation and characterization of PEG-*b*-PLA NPs

After determining the polymer concentration according to Equation (1), a few microliters of the synthesized block copolymer solution were taken out and diluted with DMF to a 1 mL solution with a concentration of 10 mg/mL. Next, water was added into the solution at a constant rate (1 mL/h) via a syringe pump under stirring at 700 rpm. When the time reached 25 min (corresponding to volumetric water content of 29%), the pump was manually stopped, and the dispersion was stirred for several additional minutes.

The obtained cloudy solution was directly transferred to a prehydrated dialysis tube (MWCO: 12–14 kDa). Dialysis was performed against precooled water at 4°C for 24 h with frequent water changes. After dialysis, the resulting solution was taken from the dialysis tube and stored in a glass vial at 4°C. The NPs were characterized using DLS, SEM, dry-TEM, and cryo-TEM techniques.

2.3.4 | Preparation and characterization of PEG-*b*-PLA polymersomes

To demonstrate that the morphology of solid PEG-*b*-PLA NPs is distinct from that of vesicles, PEG-*b*-PLA polymersomes were prepared as a control. The polymersomes were fabricated according to previous literature procedures.[6] Briefly, 10 mg of PEG-*b*-PLA was dissolved in 1 mL of organic solvent—a mixture of THF and dioxane (4:1 v/v). Next, water was added into the solution at a constant rate (1 mL/h) via a syringe pump under stirring at 700 rpm. When the time reached 60 min (corresponding to volumetric water content of 50%), the pump was manually stopped, and the dispersion was stirred for several additional minutes.

The obtained cloudy solution was directly transferred to a prehydrated dialysis tube (MWCO: 12–14 kDa). Dialysis was performed against precooled water at 4°C for 24 h with frequent water changes. After dialysis, the resulting solution was taken from the dialysis tube and stored in a glass vial at 4°C. The polymersomes were characterized using DLS, SEM, and Cryo-TEM techniques.

2.3.5 | Rapamycin encapsulation and in vitro release

Rapamycin-loaded PEG-*b*-PLA NPs were prepared in a similar manner to the unloaded NPs, except that rapamycin (2 wt% with respect to $Conc_{PEG-b-PLA}$) was added prior to self-assembly. After dialysis, residual rapamycin was removed by centrifugation. To determine the rapamycin release behavior, the rapamycin-loaded NPs were buffer exchanged from water to phosphate-buffered saline (PBS) buffer at different pH values (pH 7.4/pH 6.5/pH 5.0) before release. For the release experiments, 900 μL of each solution was transferred into a 1.5 mL microcentrifuge tube. The tubes were put on a Thermoshaker for a 120 hour test period (37°C, 500 rpm). At each designated time interval, 400 μL of supernatant was removed, and the tube was replenished with 400 μL of fresh PBS buffer (pH 7.4/pH 6.5/pH 5.0). The experiments were performed in triplicate ($N = 3$). For the analysis of rapamycin release that is, the rapamycin content in the supernatant, details can be found below.

2.3.6 | Analysis of rapamycin content

GPC was used to determine the rapamycin content in all samples. A calibration curve was prepared by injecting different volumes of a rapamycin stock solution (10 μg/mL in THF) (Figure S14a). For the analysis of rapamycin content in each supernatant sample, samples (400 μL each) were first lyophilized and redissolved in 600 μL THF, followed by vortexing. The solution was centrifuged for 5 min to pellet the PBS salts. Then, 550 μL solution was carefully taken from the sample and loaded in a GPC vial. Measurements were performed twice by injecting 20 μL each time. Acquired data were analyzed using LC solutions software, by determining the area of the UV signal peak of rapamycin (absorption at 278 nm) for both standards and samples, allowing accurate determination of the rapamycin content.

The encapsulation efficiency (EE) of rapamycin in PEG-*b*-PLA NPs was calculated according to the following equation:

$$EE\,(\%) = \frac{W_{\text{encapsulated rapamycin}}}{W_{\text{initially added rapamycin}}} \times 100\% \qquad (2)$$

with $W_{\text{encapsulated rapamycin}}$ the weight of loaded rapamycin in PEG-*b*-PLA NPs, $W_{\text{initial added rapamycin}}$ the weight of

initially added rapamycin with PEG-*b*-PLA block copolymer.

The loading capacity (LC) of rapamycin in PEG-*b*-PLA NPs was calculated according to the following equation:

$$LC\,(mg/g) = \frac{W_{\text{encapsulated rapamycin}}}{W_{\text{PEG}-b-\text{PLA in NPs}}} \quad (3)$$

with $W_{\text{encapsulated rapamycin}}$ the weight (mg) of loaded rapamycin in PEG-*b*-PLA NPs, $W_{\text{PEG}-b-\text{PLA in NPs}}$ the weight (g) of PEG-*b*-PLA block copolymer in NPs.

2.3.7 | Analysis of polymer concentration

GPC was used to determine the polymer concentration in all samples. A calibration curve was prepared by injecting different volumes of a polymer stock solution (10 mg/mL in THF) (Figure S14b). For the analysis of polymer content in each sample, 300 μL of the sample was first lyophilized and redissolved in 600 μL THF followed by vortexing. The solution was centrifuged for 5 min to pellet the PBS salts. Then, 550 μL solution was carefully taken from the sample and loaded in a GPC vial. Measurements were performed twice by injecting 20 μL each time. Acquired data were analyzed using LC solutions software, by determining the area of the RI signal peak of the polymer for both standards and samples, allowing accurate determination of the polymer concentration.

2.3.8 | Peripheral blood lymphocyte isolation

Peripheral blood mononuclear cells (PBMCs) were isolated from healthy donor-derived buffy coats (Sanquin) by density gradient centrifugation (Lymphoprep; STEMCELL Technologies). In advance, informed consent was obtained from every individual blood donor. Peripheral blood lymphocytes (PBLs) were enriched from PBMCs by monocyte adherence for 1 h at 37°C/5% CO_2 and subsequent collection of suspension cells (i.e., PBLs).

2.3.9 | CellTrace violet staining

For cell proliferation tracking, PBLs were stained with CellTrace Violet (CTV; Thermo Fisher Scientific). The cells were diluted to 1×10^6 cells/mL in PBS supplemented with 1% fetal bovine serum (FBS), mixed with an equal volume (1:1 v/v) of 5 μM CTV in PBS and

incubated for 10 min at 37°C/5% CO_2, before an equal volume (1:1:1 v/v/v) of FBS was added. The cells were then incubated for 30 min at 37°C/5% CO_2 and washed twice with X-VIVO medium (Lonza Bioscience).

2.3.10 | Preparation and characterization of sulfo-Cyanine5 (Cy5)-labeled rapamycin-loaded PEG-*b*-PLA NPs

To study the interaction behavior of rapamycin-loaded NPs with PBLs, NPs were labeled with a fluorescent dye Cy5. In short, rapamycin-loaded N_3-PEG-*b*-PLA NPs were prepared in a similar manner to rapamycin-loaded PEG-*b*-PLA NPs, except that a combination of PEG-*b*-PLA (95 wt%) and N_3-PEG-*b*-PLA (5 wt%) was used for self-assembly. Here, the addition of the azide group allows the attachment of DBCO-dye to the NPs via a strain-promoted azide-alkyne cycloaddition (SPAAC) reaction. After dialysis and removal of residual rapamycin, 200 μL solution (polymer concentration = 2.3 mg/mL) was transferred into a 1.5 mL microcentrifuge tube and diluted to 900 μL with water. Finally, an aqueous solution of Cy5-DBCO (300 μL, 9 μM) was added. The tube was put on a Thermoshaker for 2 h (30°C, 300 rpm), followed by overnight incubation at room temperature on a tube rotator. After conjugation, the NPs were purified using extensive centrifugation.

The final dye concentration on the NP surface was determined using a microplate reader. For these measurements, samples were loaded in a Thermo Fisher Scientific Nunclon 384 Flat Black plate. To calculate the concentration of conjugated Cy5, a calibration curve of fluorescence intensity versus Cy5 concentration was used. All samples and standards were measured in triplicate, with a final volume of 50 μL per well. Cy5 was excited at 635 nm, and emission was detected at 685 nm (bandwidth 20 nm, respectively). The final dye concentration on the NP surface was calculated to be 0.33 μM. Similarly, Cy5-labeled unloaded N_3-PEG-*b*-PLA NPs were prepared.

2.3.11 | T cell suppression assay

To examine the effects of rapamycin-loaded NPs on the suppression of T cell proliferation, 5×10^5 PBLs/well in a 96-well U-bottom plate were stimulated with Dynabeads (1:2 cell/bead; Thermo Fisher Scientific) in the presence of either free rapamycin, rapamycin-loaded NPs or unloaded NPs. For the first two groups, three different rapamycin concentrations (10^{-5}, 10^{-3}, and

10^{-1} μM) were used, respectively; for the unloaded NP group, three different polymer concentrations were used, and these concentrations corresponded to the three polymer concentrations in the rapamycin-loaded NP group, respectively. For each condition, PBLs from four donors ($N = 4$) were used. Subsequently, PBLs were cultured in X-VIVO medium at 37°C/5% CO_2 for 90 h, and the proliferation of T cells were assessed with flow cytometry.

2.3.12 | Flow cytometry

For flow cytometric analysis, the following antibodies were purchased from BioLegend: CD3-FITC (clone OKT3), CD4-APC/Cy7 (clone RPA-T4), CD8-PerCP (clone SK1). Dead cells were stained using the Zombie Yellow Fixable Viability Kit (BioLegend) according to the manufacturer's protocol. Staining was performed either in PBS or PBS supplemented with 0.1% BSA, 0.05% sodium azide, and 1 mM EDTA. Fluorescence was measured using a BD FACSymphony A3 Cell Analyzer (BD Biosciences) and data was analyzed using FlowJo 10.9.0 software (Tree Star).

2.3.13 | Internalization of Cy5-labeled rapamycin-loaded PEG-*b*-PLA NPs in PBLs

To support the internalization of NPs, PBLs were seeded in a 96-well U-bottom plate (5×10^5 PBLs/well) and incubated with Cy5-labeled rapamycin-loaded PEG-*b*-PLA NPs (rapamycin concentration = 10^{-1} μM) at 37°C/5% CO_2 for 12 h. Subsequently, the cell membrane was stained with BioTracker 490 Green Cytoplasmic Membrane Dye for 20 min using the manufacturer's protocol. Fluorescence images were acquired using confocal laser scanning microscopy (CLSM; Leica TCS SP5X) for live cell imaging.

2.3.14 | Statistical analysis

Data are presented as the mean ± standard deviation (SD). All *p* values were two-tailed, and $p < 0.05$ was considered significant. Data were analyzed by one-way (pH as the factor determining rapamycin release) or two-way (rapamycin concentration and delivery method as the two factors determining T cell suppression) analysis of variance (ANOVA). Multiplicity adjusted p-values were calculated using the Tukey correction for multiple comparison. Statistical tests were performed using Prism 10.0.1 software (GraphPad Software).

3 | RESULTS AND DISCUSSION

3.1 | Synthesis and characterization of PEG-*b*-PLA block copolymer

The synthesis of PEG-*b*-PLA block copolymer was performed by a ring-opening polymerization reaction using α-methoxy-ω-hydroxy polyethylene glycol (mPEG$_{22}$) as the initiator, $_{D,L}$-lactide (45 equiv.) as the monomer, dry DMF as the solvent and 1,8-diazabicyclo(5.4.0)undec-7-ene (DBU) as the catalyst (Figure S1a). First, the monomer concentration was optimized to achieve maximum monomer conversion based on proton nuclear magnetic resonance (^{1}H-NMR) measurements. When 0.3 and 0.5 M were applied as the monomer concentration, the monomer conversion only reached 56% and 76% after 16 h, respectively (Figure S1b,c). When the monomer concentration was raised to 0.8 M, the conversion increased significantly to 95% within 4 h (Figure S1d). Compared to the previously reported synthesis of PEG-*b*-PLA, with similar composition under the same conditions, but in dry DCM,[6,25] the synthesis in dry DMF required an increased monomer concentration and a prolonged reaction time to achieve a high monomer conversion (>90%), demonstrating the negative impact of DMF on the polymerization rate. A similar observation has been previously reported, where the rate of the ring-opening polymerization of ε-caprolactone was found to be delayed when DMF was used as the solvent, likely due to interactions between DMF and the metal catalyst.[26] Correspondingly, considering the mechanism of DBU-catalyzed ring-opening polymerization of lactide in our case,[27] a plausible explanation could be an undesired interaction between DMF and DBU, as has been shown before,[28,29] weakening the activation of the initiator, and thus affecting the polymerization to some extent. Nevertheless, with a higher monomer concentration in our case (0.8 M), the polymerization proceeded to a high conversion even though it required a relatively long time.

To investigate the quality of the synthesized polymer, the PEG-*b*-PLA solution was first dialyzed against water to remove all organic solvent and then lyophilized overnight. The degree of polymerization, as calculated by ^{1}H NMR spectroscopy, using the methylene protons of mPEG$_{22}$ and the methine protons of PLA, was 43 (Figure S2a; hydrophilic PEG weight fraction $f = 14\%$). No minor peaks corresponding to impurities were observed. The GPC trace showed that the polymer eluted after 15 min, with dispersity (Đ) of 1.2, indicating that the block copolymer had a relatively narrow molecular weight distribution, highlighting that the ring-opening polymerization process was well controlled (Figure S2b). It can therefore be concluded that DMF as

the solvent did not bring clear adverse effects other than slowing the reaction rate down. Remarkably, this method yielded pure PEG-*b*-PLA, allowing the time-consuming polymer purification process to be skipped and self-assembly to begin directly.

3.2 | Investigation of PEG-*b*-PLA self-assembly and characterization of PEG-*b*-PLA NPs

Having synthesized and characterized the PEG-*b*-PLA block copolymer, we investigated the effect of water content (C_w) on its self-assembly. After determining the polymer concentration according to Equation (1), the solution of PEG-*b*-PLA was first diluted with DMF to a concentration of 10 mg/mL. Next, different volumes of water were added to 1 mL of the polymer solution at a constant rate (1 mL/h) via a syringe pump, respectively. Correspondingly, a series of solution turbidities were recorded (Figure 2A). Normally, for particle assembly via a solvent switch method, that is, mixing water (a partial non-solvent) and organic solution of amphiphilic polymers, the curve of turbidity versus C_w only shows an increase upon reaching the critical water content.[30–33] Indeed, such behavior was observed when the self-assembly of PEG-*b*-PLA copolymers was performed under the same solvent switch conditions, when THF and dioxane (4:1 v/v) were used instead of DMF (Figure S3). When DMF was used, however, three different turbidity regimes were observed (Figure 2A): (i) a rapid increase, starting from C_w of ca. 15 vol% until approximately 30 vol%, indicating progress in microphase separation of the solution and self-assembly of the copolymer;[34] (ii) a rather slow increase between C_w 30 and 40 vol%; (iii) a sudden drop in turbidity beyond C_w 40 vol %. Clearly, the change in turbidity upon increasing water:DMF ratios, is distinct from a typical NP assembly turbidity curve. Such an unusual drop is significant and could not be a consequence of a dilution effect,[33] but, rather, can be a result of a morphological transition.[35–38] These findings suggest conditions with water vol% ranging from 20 to 40 vol% C_w, at which particle formation can be controlled. In particular, approximately 30 vol% was found to be an ideal C_w for reproducible PEG-*b*-PLA NP formation; therefore, this parameter was chosen for self-assembly in the following experiments.

Next, PEG-*b*-PLA NPs were prepared by self-assembly, followed by dialysis against water to remove DMF. The average hydrodynamic diameter (D_h) of the NPs was determined to be 611 ± 10 nm (Figure 2B,C). The PDI was below 0.1, indicating that the particles had a narrow size distribution. Furthermore, using SEM, the NPs were found to have a well-defined spherical morphology (Figure 2D). It is worth mentioning that this morphology is different from PEG-*b*-PLA polymersomes prepared using the same polymer composition via THF/dioxane/water solvent mixture (4:1:5 v/v/v) (Figure S4a). As a result of the drying effect,[39] the polymersomes could not maintain their structure during water evaporation, and collapsed on the silicon wafer, resulting in a 'typical' ring-shaped structure. In contrast, under the same conditions, our formed NPs maintained their spherical structure, which strongly indicates that their internal structure is solid rather than hollow.

To test this hypothesis, we used two complementary TEM techniques, dry- and cryo-TEM microscopy, to further characterize the NPs. Both dry-TEM and cryo-TEM data (Figure 2E,F) confirmed that the formed PEG-*b*-PLA NPs are solid, which is distinct from polymersomes (Figure S4b). Although it is difficult to pinpoint the exact internal structure from the TEM images, further analysis of the intensity of a line profile across a NP (Figure S5) showed that they do not possess an interior hollow structure, which is a typical feature of multi-compartment micelles.[40–43] Instead, they were similar to large compound micelles reported previously.[44–46]

Moreover, to examine possible morphological transitions after the turbidity inflection point (C_w: 40 vol%), 43 and 50 vol% were chosen as C_w for particle formation, followed by dialysis—representative SEM images are shown in Figure S6a,b, respectively. Compared to the NPs with spherical shape and smooth surface obtained using 29 vol% as C_w, the particles shown in Figure S6a had rough surfaces and increased polydispersity, suggesting that particle integrity was compromised as a result of the addition of excess water during self-assembly, although their turbidity was similar. Besides, the average D_h of the formed NPs (C_w: 43 vol%) was 468 ± 5 nm (Figure S7), which is 20% smaller than their counterparts formed at C_w: 29 vol%. For the other sample (C_w: 50 vol %), the turbidity of the solution was reduced to about 10% compared to the highest value, suggesting a (nearly) complete disintegration of the particles. However, in this case, the large NPs were still observed after dialysis (Figure S6b). The average D_h of the NPs was 547 ± 3 nm (Figure S7), which is even larger than those formed using 43 vol% as C_w. A plausible explanation to this observation is possible particle aggregation and precipitation as the system was driven to reduce the thermodynamic penalty caused by the unfavorable interaction between water and PLA chains, leading to a significant reduction in turbidity.

For biomedical applications, one concern is whether DMF can be efficiently removed by dialysis. DMF is a toxic chemical, known to cause irritation and damage to

the eyes and liver.[47] According to the International Council for Harmonization of Technical Requirements for Registration of Pharmaceuticals for Human Use (ICH) guideline, DMF is classified as a Class II solvent and the permitted concentration limit for DMF is set to 880 ppm. In this study, the residual DMF content was determined by gas chromatography with flame ionization detection (GC-FID) technique (Figure S8). Water and DMF in water (1000 ppm, for ease of preparation) were used as negative and positive controls, respectively. After dialysis, 1 mL of the NP solution (ca. 2.3 mg/mL) was centrifuged, and neither the supernatant nor the resuspension of the NPs showed any visible characteristic peaks of DMF. The peaks appeared only after the particles were disintegrated by heating, however, the peak area was approximately 60 times significantly smaller than that of the positive control, which showed the DMF concentration was much lower than the limit of 880 ppm, indicating the effectiveness of dialysis to remove DMF. Since the residual DMF content in the NPs did not exceed the permitted concentration limit, they can serve as a potential candidate for biomedical applications.

To determine whether the dialysis time (24 h) could be shortened, we set up control experiments to look into the residual DMF content in the dialysis bag after 2, 4, and 8 h (Figure S9). Although the DMF content was higher than the 1000 ppm standard after 2 h, it was clear that the content could be considered below the permitted concentration limit after 4 h of dialysis. Additionally, no catalyst or monomer was detected at NMR-visible levels.

3.3 | Rapamycin encapsulation and in vitro release

In this study, rapamycin was selected as a model immunosuppressive drug for encapsulation in PEG-*b*-PLA NPs and release in PBS buffer, to demonstrate the potential drug loading and delivery capacities of our PEG-*b*-PLA NP platform.

Rapamycin was directly added before the PEG-*b*-PLA self-assembly process at a concentration of 2 wt% with respect to $Conc_{PEG-b-PLA}$. Non-loaded rapamycin was removed by dialysis and centrifugation. After purification, the NPs were found to retain their well-defined spherical morphology (Figure S10). DLS measurements confirmed that the particle size distribution remained narrow (PDI < 0.1), and the average D_h of the NPs in neutral PBS buffer was determined to be 618 ± 10 nm (Figure S11). Zeta potential (ζ) measurements indicated that the loading of rapamycin did not have a significant effect on the surface charge of the NPs (Table S1). In addition, according to Equations (2) and (3), the
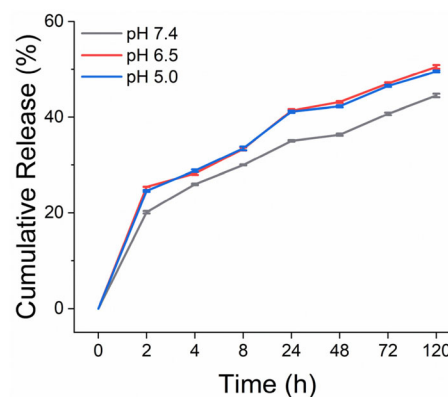
FIGURE 3 Cumulative release of rapamycin from PEG-*b*-PLA nanoparticles (NPs) in PBS buffer (pH 7.4/pH 6.5/pH 5.0) at 37°C for 120 h. Data are presented as the mean $\pm$ SD ($N = 3$).

encapsulation efficiency (EE) and loading capacity (LC) of rapamycin in PEG-*b*-PLA NPs were calculated to be 22% and 6.6 mg/g of polymer respectively, based on chromatography measurements.

To investigate the potential of PEG-*b*-PLA NPs for drug delivery, we studied the release performance of rapamycin-loaded NPs under different pHs (pH 7.4/pH 6.5/pH 5.0) in PBS. At each designated time interval, the quantity of released rapamycin was calculated using GPC-UV measurements. The drug release was monitored for 120 h, and the release profiles are shown in Figure 3. After 2 h, the NPs exhibited a burst release behavior of around 25% at acidic pHs, which was 5% higher than at neutral pH. Yet, the release was slower over the following period of time, and the cumulative release values for the three groups were ca. 45%, 51%, and 50%, for pH 7.4, 6.5, and 5.0, respectively, after 5 days. The rapamycin-loaded NPs showed sustained drug release under all three conditions, although there was a statistically significant difference between the final cumulative release value at neutral pH and those at acidic pHs ($p < 0.0001$), the release profiles were comparable and the difference (ca. 5% after 5 days) was practically insignificant, indicating that the release performance was not markedly influenced by the pH.

Generally, two factors are known to govern the drug release kinetics from biodegradable polymeric NPs: (i) diffusion of the drug through the NP matrix; (ii) degradation of the NP matrix, with poration and disintegration being typical examples (at different time points).[48] These two factors normally govern the process and influence each other. To understand the release mechanism and determine which factor is the main driver of drug release from our NP platform, it is necessary to compare the contributions of drug diffusion and matrix degradation. The diffusion behavior depends on

many characteristics of the system. More specifically, for drug-loaded PEG-*b*-PLA NPs, these characteristics include the properties of PEG-*b*-PLA polymer, such as molecular weight, chain lengths of PEG and PLA, and PEG/PLA ratio; the properties of the drug, such as hydrophilicity/hydrophobicity; the drug distribution over the matrix; and the interaction between the drug and the matrix.[3] Therefore, drug diffusion is actually case-dependent and difficult to be explained with a unified model. In contrast, degradation of the NP matrix can be more easily determined and simply explained by two main mechanisms according to the driving force:

(a) bulk-erosion induced by polymer-chain cleavage; (b) surface-erosion mediated by other factors, while the polymer remains nearly stable.[49]

For PEG-*b*-PLA polymer, the hydrophobic block, i.e., PLA, can undergo chain cleavage due to hydrolysis and scission of ester bonds, and this process can be accelerated at acidic pH compared to neutral pH.[50] However, in previously reported literature, depending on the characteristics of the system, such as the nature of PEG-*b*-PLA copolymers and their packing in the formed NPs, the results were inconsistent as to whether the cleavage under different pH conditions made a significant

TABLE 1 NP characterization by polymer analysis after rapamycin release in PBS buffer (pH 7.4/pH 6.5/pH 5.0) at 37°C for 120 h.

Results (normalized)	Day 0	Day 5		
	pH 7.4 (%)	pH 7.4 (%)	pH 6.5 (%)	pH 5.0 (%)
Lactide units	100	+4.31	−0.72	−4.31
Mn		−1.01	+1.20	+1.04
Polymer conc		−50.59	−53.64	−56.14

Note: Before gel permeation chromatography (GPC) measurements, the NP solutions were freeze-dried and dissolved in THF, therefore, they were in the free polymer form. Since the number of lactide units and Mn were almost the same as those of PEG-*b*-PLA, the polymer concentration that is, the integration of the polymer peak, can be used as the indicator for particle weight loss after release. All values were normalized to the initial values in PBS buffer (pH 7.4) before release. Data are presented as the mean ($n = 4$) for Mn and polymer concentrations.
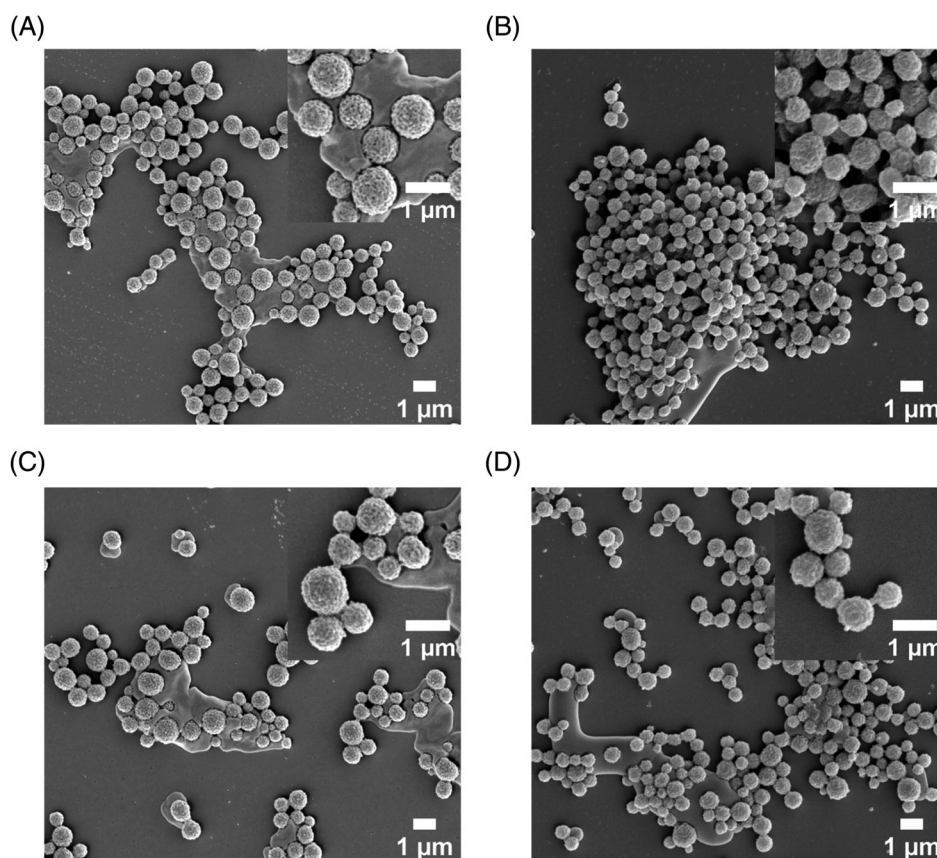
FIGURE 4 Rapamycin-loaded PEG-*b*-PLA NP erosion after incubation in PBS. Representative scanning electron microscopy (SEM) images of the NPs at (A) Day 2 and (B) Day 5 in PBS buffer (pH 7.4); (C) Day 2 and (D) Day 5 in PBS buffer (pH 6.5).
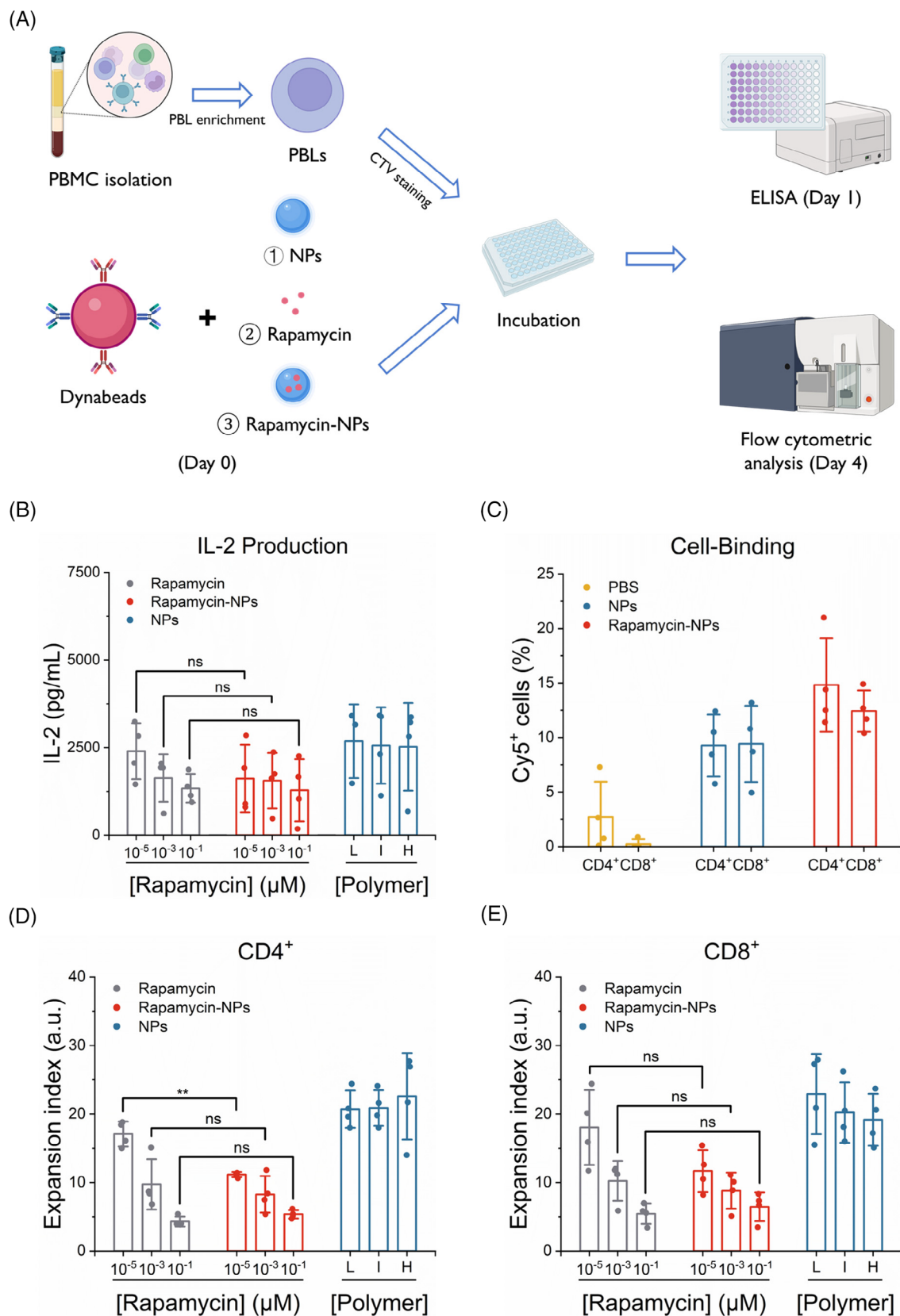
FIGURE 5 Legend on next page.

difference in drug release within a short period (<5 days). For example, the differences were observed in some studies,[51–53] while in others, PEG-*b*-PLA NPs exhibited similar release profiles at acidic pH and neutral pH.[54–58]

In our study, to determine the possible hydrolysis of PEG-*b*-PLA after drug release, NMR spectroscopy and GPC techniques were used to analyze the number of lactide units in the polymer and the number average molecular weight (Mn) of the polymer, respectively. Furthermore, the polymer concentration was calculated and included in Table 1.

It is clear from the data in Table 1 that after 5 days, neither the number of lactide units in the polymer nor its Mn were significantly different among the three groups. This finding suggests that the cleavage of PEG-*b*-PLA was not affected much under acidic pH conditions, possibly due to the compact packing of the polymer chains and consequent slow rate of hydrolysis. This effect can be ascribed to the fact that the packing of PEG and PLA blocks in the micellar-like structure restrains the diffusion/permeation rate of the buffer through the matrix, thus reducing their interaction. However, there was a significant decrease in polymer concentration in all three groups, by more than 50% after 120 h, showing that the degradation of the NP matrix occurred in preference to notable polymer hydrolysis. The evidence supports that the degradation of the particles might be primarily driven by surface erosion.

To visualize the degradation of rapamycin-loaded NPs in PBS buffer at different pH values (7.4 or 6.5), a small aliquot was taken from each sample after 2 and 5 days, respectively. Representative SEM images of the samples are shown in Figure 4. Before drug release, the particles showed a narrow size distribution as well as a smooth surface (Figure S10). After 2 days, in both groups, the NPs were surface-porated, while retaining their spherical shape. After 5 days, the NPs increased their surface-roughness and were no longer spherical. In addition, DLS measurements were carried out to determine the particle size distribution (PSD) of the NPs after rapamycin release (Figure S12). After 120 h, the average D_h of the NPs in all three groups increased to above 1 μm and the PDI was higher compared to that before drug release, which might be a result of particle aggregation into clusters caused by the erosion.[59] Further PSD analysis (Table S2) was performed according to Figure 4. It was observed that NPs under neutral pH conditions showed more significant swelling in the early stage of release, while NPs under acidic pH conditions showed the similar behavior in the later stage. This time-independent difference will be examined in the future.

In this study, rapamycin release was determined by measuring rapamycin contents in the supernatant after centrifugation. One might argue whether the observed erosion was caused by centrifugation. To this end, the stability of rapamycin-loaded NPs to centrifugation was assessed as a control. After a series of centrifugation and resuspension, the NPs maintained a well-defined spherical morphology (Figure S13) and a nearly constant polymer concentration (Table S3), as verified by SEM and GPC measurements, respectively. Another control experiment was performed to find out whether centrifugation caused the release without affecting the integrity of the NPs. After centrifugation (time = 0 h), we did observe rapamycin in the supernatant. However, the integration value was approximately 1000 times lower than that of loaded rapamycin. From our perspective, this extremely low release is negligible compared to the release caused by the degradation of the NP matrix.

3.4 | In vitro T cell suppression

The immunosuppressive drug rapamycin has been shown to inhibit T cell proliferation by blocking the mammalian target of the rapamycin (mTOR) signaling pathway.[60] As a proof-of-concept that our rapamycin-loaded NPs can suppress T cell proliferation, we tested the in vitro

FIGURE 5 In vitro T cell suppression studies. (A) Experimental design. Peripheral blood mononuclear cells (PBMCs) were isolated from healthy donor-derived buffy coats by density gradient centrifugation, followed by peripheral blood lymphocyte (PBL) enrichment through monocyte adherence. After CellTrace Violet (CTV) staining, cells were stimulated with Dynabeads (1:2 cell/bead) in the presence of either free rapamycin, rapamycin-loaded PEG-*b*-PLA nanoparticles (NPs), or unloaded NPs. After 24 h (i.e., Day 1), the supernatants were collected and analyzed by IL-2 ELISA analysis. After 90 h (i.e., Day 4), the cells were assessed by flow cytometry. (B) Production of IL-2 determined through ELISA after 24 h. (C) Binding of rapamycin-loaded NPs or unloaded NPs to CD4^{+} and CD8^{+} T cells (%) as determined through flow cytometric analysis of Cy5 fluorescence after 90 h. Expansion index (average fold-expansion of the whole population) of (D) CD4^{+} and (E) CD8^{+} T cells as determined through flow cytometric analysis of CTV fluorescence after 90 h. The three polymer concentrations in the unloaded NP group corresponded to the three polymer concentrations in the rapamycin-loaded NP group, respectively: H, high concentration; I, intermediate concentration; L, low concentration. All data are represented as the mean ± SD ($N = 4$ donors); ns: $p > 0.05$, **: $p < 0.01$.

proliferation of activated PBLs ($N = 4$ donors) incubated with three concentrations of either unloaded NPs, free rapamycin or rapamycin-loaded NPs (Figure 5A). After 24 h, ELISA analysis showed that both free and loaded rapamycin reduced the production of IL-2 in comparison with the unloaded NPs (Figure 5B). Since IL-2 is mainly produced by activated CD4$^+$ T cells, the results suggest that the activation was inhibited, demonstrating that the loaded rapamycin was released and utilized. After 90 h, flow cytometric analysis (Figure S15a) revealed significant binding of Cy5-labeled NPs to both CD4$^+$ and CD8$^+$ T cell subsets (Figures 5C and S15b). Since there is no antigen presented on the surface of the NPs, this binding behavior can be explained by the fact that they are actually internalized by T cells rather than bound to T-cell receptors. To support the internalization of NPs, in addition to flow cytometric analysis, we performed fluorescence image analysis of NPs in live PBLs using CLSM. This was confirmed as Cy5-labeled NPs were found to be localized within cells (Figure S16). Additionally, it was shown that PEG-*b*-PLA NPs did not reduce cell viability upon an increase in rapamycin concentration (Figure S15c). This data suggests that PEG-*b*-PLA NPs associate with T cells in vitro without inducing significant cytotoxicity and could be a safe platform for the delivery of rapamycin. Furthermore, both free and loaded rapamycin inhibited T cell expansion in a concentration-dependent manner for both CD4$^+$ ($p < 0.0001$) and CD8$^+$ ($p = 0.0001$) T cell subsets (Figure 5D,E). Interestingly, rapamycin-loaded PEG PLA NPs compared to free drug suppressed T cell expansion more strongly in CD4$^+$ T cells ($p = 0.0207$) than in CD8$^+$ T cells ($p = 0.1008$). A further group-to-group analysis of the same drug concentration showed that the encapsulation effect was significant at the lowest rapamycin concentration for CD4$^+$ cells ($p = 0.0074$) but not for CD8$^+$ cells ($p = 0.1010$) (Figure 5D,E). Similar concentration-dependent results were observed for the mean number of divisions undergone by the T cells (Figure S15d,e), but in spite of the different effects on CD4$^+$ and CD8$^+$ T cell proliferation, no significant differences were found in the CD4 over CD8 ratio (Figure S14f). Moreover, rapamycin more strongly suppressed CD4$^+$ T cells which could be explained by the higher frequency of CD4$^+$ T cells generally found in PBLs (Figure S14f). Taken together, these data demonstrate that rapamycin is capable of suppressing in vitro T cell proliferation, and its encapsulation in PEG-*b*-PLA NPs does not impair this effect and even enables it to perform better on CD4$^+$ cells at low rapamycin concentration. Given the sustained-release effect provided by the encapsulation, rapamycin-loaded PEG-*b*-PLA NPs would be a more suitable candidate for systemic administration than the free drug.

4 | CONCLUSIONS

In this work, a novel and facile method for the preparation of PEG-*b*-PLA NPs was achieved through a sequential two-step process, involving synthesis of PEG-*b*-PLA in DMF, directly followed by water addition to the polymer solution. By a combination of DLS, SEM, dry- and cryo-TEM techniques, these NPs were shown to be well-defined spherical and possess a solid structure. Furthermore, the potential drug delivery capacity of the PEG-*b*-PLA NPs was investigated by rapamycin encapsulation and release testing. In vitro drug release tests showed that rapamycin-loaded NPs had comparable sustained-release profiles at different pH conditions, which could be elucidated by the similarity in the degradation behavior of the NP matrix after release. Moreover, in vitro T cell suppression assays revealed that rapamycin-loaded NPs exhibited similar or even better inhibitory performance to free rapamycin on CD4$^+$ and CD8$^+$ cells at three rapamycin concentrations, showing that the encapsulation does not compromise the suppression effect.

To the best of our knowledge, apart from ring-opening polymerization-induced crystallization-driven self-assembly (ROPI-CDSA),[17] this is the first example to show that PEG-*b*-PLA synthesis and particle formation can be combined in a continuous manner. This method does not require polymer purification between polymer synthesis and particle formation, which is considered necessary in conventional studies, in order to maximize preparation efficiency. This study could contribute to a scalable synthesis of polymeric NPs. For example, the approach can be applied to the fabrication of other polymeric particles by polymer synthesis in DMF or other water-miscible organic solvents and water-induced self-assembly. It can also be used in microfluidic-based platforms for continuous NP fabrication. In addition, the pH-independent sustained-release behavior of rapamycin from the NPs raises the possibility of this system to precisely control the therapeutic window of drugs regardless of changes in ambient pH. Overall, our rapamycin-loaded PEG-*b*-PLA NPs offer interesting properties (including straightforward synthesis, dimensions, stability, biocompatibility, and demonstrated therapeutic effect) for applications in the emergent area of immunotherapy.

CONFLICT OF INTEREST STATEMENT
The authors declare no competing financial interest.

ORCID
Yudong Li https://orcid.org/0009-0006-9140-5733
Antoni Llopis-Lorente https://orcid.org/0000-0002-6987-9506
Jan C. M. van Hest https://orcid.org/0000-0001-7973-2404
Loai K. E. A. Abdelmohsen https://orcid.org/0000-0002-0094-1893

REFERENCES
[1] N. Kamaly, Z. Y. Xiao, P. M. Valencia, A. F. Radovic-Moreno, O. C. Farokhzad, *Chem. Soc. Rev.* **2012**, *41*, 2971.
[2] M. Elsabahy, K. L. Wooley, *Chem. Soc. Rev.* **2012**, *41*, 2545.
[3] R. Z. Xiao, Z. W. Zeng, G. L. Zhou, J. J. Wang, F. Z. Li, A. M. Wang, *Int. J. Nanomed.* **2010**, *5*, 1057.
[4] B. Tyler, D. Gullotti, A. Mangraviti, T. Utsuki, H. Brem, *Adv. Drug Deliv. Rev.* **2016**, *107*, 163.
[5] B. K. Lee, Y. Yun, K. Park, *Adv. Drug Deliv. Rev.* **2016**, *107*, 176.
[6] L. K. Abdelmohsen, D. S. Williams, J. Pille, S. G. Ozel, R. S. Rikken, D. A. Wilson, J. C. van Hest, *J. Am. Chem. Soc.* **2016**, *138*, 9353.
[7] I. A. Pijpers, S. Cao, A. Llopis-Lorente, J. Zhu, S. Song, R. R. Joosten, F. Meng, H. Friedrich, D. S. Williams, S. Sánchez, *Nano Lett.* **2020**, *20*, 4472.
[8] T. F. Burton, J. Pinaud, O. Giani, *Macromolecules* **2020**, *53*, 6598.
[9] R. Simonutti, D. Bertani, R. Marotta, S. Ferrario, D. Manzone, M. Mauri, M. Gregori, A. Orlando, M. Masserini, *Polymer* **2021**, *218*, 123511.
[10] H. Jeffery, S. Davis, D. O'hagan, *Int. J. Pharm.* **1991**, *77*, 169.
[11] G. Ruan, S.-S. Feng, Q.-T. Li, *J. Control. Release* **2002**, *84*, 151.
[12] G. Ruan, S.-S. Feng, *Biomaterials* **2003**, *24*, 5037.
[13] S. H. Kim, F. Nederberg, R. Jakobs, J. P. K. Tan, K. Fukushima, A. Nelson, E. W. Meijer, Y. Y. Yang, J. L. Hedrick, *Angew. Chem. Int. Ed.* **2009**, *48*, 4508.
[14] T. Riley, S. Stolnik, C. R. Heald, C. D. Xiong, M. C. Garnett, L. Illum, S. S. Davis, S. C. Purkiss, R. J. Barlow, P. R. Gellert, *Langmuir* **2001**, *17*, 3168.
[15] N. J. Penfold, J. Yeow, C. Boyer, S. P. Armes, *ACS Macro Lett.* **2019**, *8*, 1029.
[16] C. Liu, C.-Y. Hong, C.-Y. Pan, *Polym. Chem.* **2020**, *11*, 3673.
[17] P. J. Hurst, A. M. Rakowski, J. P. Patterson, *Nat. Commun.* **2020**, *11*, 1.
[18] Q. Q. Shi, Y. B. Chen, J. J. Yang, J. Yang, *Chem. Commun.* **2021**, *57*, 11390.
[19] B. D. Kahan, J. S. Camardo, *Transplantation* **2001**, *72*, 1181.
[20] D. Fantus, N. M. Rogers, F. Grahammer, T. B. Huber, A. W. Thomson, *Nat. Rev. Nephrol.* **2016**, *12*, 587.
[21] J. Ochando, Z. A. Fayad, J. C. Madsen, M. G. Netea, W. J. Mulder, *Am. J. Transplant.* **2020**, *20*, 10.
[22] A. Haeri, M. Osouli, F. Bayat, S. Alavi, S. Dadashzadeh, *Artificial Cells Nanomed. Biotechnol.* **2018**, *46*, 1.
[23] W. J. Mulder, J. Ochando, L. A. Joosten, Z. A. Fayad, M. G. Netea, *Nat. Rev. Drug Discov.* **2019**, *18*, 553.
[24] J. Schindelin, I. Arganda-Carreras, E. Frise, V. Kaynig, M. Longair, T. Pietzsch, S. Preibisch, C. Rueden, S. Saalfeld, B. Schmid, J. Y. Tinevez, D. J. White, V. Hartenstein, K. Eliceiri, P. Tomancak, A. Cardona, *Nat. Methods* **2012**, *9*, 676.
[25] A. C. Wauters, I. A. Pijpers, A. F. Mason, D. S. Williams, J. Tel, L. K. Abdelmohsen, J. C. van Hest, *Biomacromolecules* **2018**, *20*, 177.
[26] Y. Robinson, *J. Chem. Res. Synop.* **1999**, *7*, 452.
[27] N. J. Sherck, H. C. Kim, Y.-Y. Won, *Macromolecules* **2016**, *49*, 4699.
[28] J. Muzart, *Tetrahedron* **2009**, *65*, 8313.
[29] R. Ramirez-Jimenez, M. Franco, E. Rodrigo, R. Sainz, R. Ferritto, A. Lamsabhi, J. L. Acena, M. B. Cid, *J. Mater. Chem. A* **2018**, *6*, 12637.
[30] H. Shen, A. Eisenberg, *J. Phys. Chem. B* **1999**, *103*, 9473.
[31] A. Choucair, A. Eisenberg, *Eur. Phys. J. E: Soft Matter Biol. Phys.* **2003**, *10*, 37.
[32] Z. L. Zhuang, C. H. Cai, T. Jiang, J. P. Lin, C. Y. Yang, *Polymer* **2014**, *55*, 602.
[33] J. G. Xiao, J. Z. Du, *J. Am. Chem. Soc.* **2020**, *142*, 6569.
[34] L. F. Zhang, H. W. Shen, A. Eisenberg, *Macromolecules* **1997**, *30*, 1001.
[35] I. Weitzhandler, M. Dzuricky, I. Hoffmann, F. G. Quiroz, M. Gradzielski, A. Chilkoti, *Biomacromolecules* **2017**, *18*, 2419.
[36] S. G. Wu, Q. Zhang, Y. Deng, X. Li, Z. Luo, B. Zheng, S. Y. Dong, *J. Am. Chem. Soc.* **2020**, *142*, 448.
[37] T. J. Neal, N. J. W. Penfold, S. P. Armes, *Angew. Chem. Int. Edit.* **2022**, *61*, e202207376.
[38] G. Bovone, L. Cousin, F. Steiner, M. W. Tibbitt, *Macromolecules* **2022**, *55*, 8040.
[39] C. K. Wong, M. H. Stenzel, P. Thordarson, *Chem. Soc. Rev.* **2019**, *48*, 4019.
[40] J. Z. Du, S. P. Armes, *Soft Matter* **2010**, *6*, 4851.
[41] B. E. McKenzie, F. Nudelman, P. H. H. Bomans, S. J. Holder, N. A. J. M. Sommerdijk, *J. Am. Chem. Soc.* **2010**, *132*, 10256.
[42] D. Daubian, J. Gaitzsch, W. Meier, *Polym. Chem.* **2020**, *11*, 1237.
[43] S. Lin, F. Y. Wang, J. Z. Du, *Polym. Chem.* **2021**, *12*, 3362.
[44] L. F. Zhang, A. Eisenberg, *Science* **1995**, *268*, 1728.
[45] L. F. Zhang, A. Eisenberg, *J. Am. Chem. Soc.* **1996**, *118*, 3168.
[46] P. Bhargava, Y. F. Tu, J. X. Zheng, H. M. Xiong, R. P. Quirk, S. Z. D. Cheng, *J. Am. Chem. Soc.* **2007**, *129*, 1113.
[47] F. Lamkarkach, M. Meslin, M. Kolossa-Gehring, P. Apel, R. Garnier, *Toxics* **2022**, *10*, 298.
[48] K. S. Soppimath, T. M. Aminabhavi, A. R. Kulkarni, W. E. Rudzinski, *J. Control. Release* **2001**, *70*, 1.
[49] A. Belbella, C. Vauthier, H. Fessi, J. P. Devissaguet, F. Puisieux, *Int. J. Pharm.* **1996**, *129*, 95.
[50] T. Ivanova, I. Panaiotov, F. Boury, J. E. Proust, J. P. Benoit, R. Verger, *Colloid Surface B* **1997**, *8*, 217.
[51] F. Ahmed, R. I. Pakunlu, G. Srinivas, A. Brannan, F. Bates, M. L. Klein, T. Minko, D. E. Discher, *Mol. Pharm.* **2006**, *3*, 340.

[52] G. Y. Wang, D. Maciel, Y. L. Wu, J. Rodrigues, X. Y. Shi, Y. Yuan, C. S. Liu, H. Tomas, Y. L. Li, *ACS Appl. Mater. Interfaces* **2014**, *6*, 16687.

[53] Y. Cai, Z. M. Xu, Q. Shuai, F. T. Zhu, J. Xu, X. Gao, X. R. Sun, *Biomater. Sci.* **2020**, *8*, 2274.

[54] H. Mei, W. Shi, Z. Q. Pang, H. F. Wang, W. Y. Lu, X. G. Jiang, J. Deng, T. Guo, Y. Hu, *Biomaterials* **2010**, *31*, 5619.

[55] Z. Zhang, X. F. Chen, L. Chen, S. J. Yu, Y. Cao, C. L. He, X. S. Chen, *ACS Appl. Mater. Interfaces* **2013**, *5*, 10760.

[56] L. Xiao, L. X. Huang, F. Moingeon, M. Gauthier, G. Yang, *Biomacromolecules* **2017**, *18*, 2711.

[57] P. L. Qi, X. H. Wu, L. Liu, H. M. Yu, S. Y. Song, *Front. Pharmacol.* **2018**, *9*, 9.

[58] Y. Chen, C. J. Yang, J. Mao, H. G. Li, J. S. Ding, W. H. Zhou, *RSC Adv.* **2019**, *9*, 11026.

[59] J. X. Shao, S. P. Cao, D. S. Williams, L. K. E. A. Abdelmohsen, J. C. M. van Hest, *Angew. Chem. Int. Edit.* **2020**, *59*, 16918.

[60] A. W. Thomson, H. R. Turnquist, G. Raimondi, *Nat. Rev. Immunol.* **2009**, *9*, 324.

SUPPORTING INFORMATION

Additional supporting information can be found online in the Supporting Information section at the end of this article.

How to cite this article: Y. Li, J. F. Scheerstra, Y. Liu, A. C. Wauters, J. Wang, H. Wu, T. Patiño, A. Llopis-Lorente, J. C. M. van Hest, L. K. E. A. Abdelmohsen, *J. Polym. Sci.* **2024**, *62*(10), 2215. https://doi.org/10.1002/pol.20230941